

1 **The metabolic cofactor Coenzyme A enhances alternative macrophage activation**
2 **via MyD88-linked signaling**

3

4 Anthony E. Jones¹, Amy Rios¹, Neira Ibrahimovic¹, Carolina Chavez^{1,2}, Nicholas A. Bayley¹,
5 Andréa B. Ball¹, Wei Yuan Hsieh², Alessandro Sammarco², Amber R. Bianchi¹, Angel A. Cortez¹,
6 Thomas G. Graeber¹, Alexander Hoffmann², Steven J. Bensinger², and Ajit S. Divakaruni^{1,3}

7

8 ¹Departments of Molecular and Medical Pharmacology, ²Microbiology, Immunology, and
9 Molecular Genetics, University of California, Los Angeles, Los Angeles, CA 90095, USA

10 ³Lead contact

11 Correspondence: adivakaruni@mednet.ucla.edu

12 Running Title: *CoA enhances alternative activation via MyD88*

13

14

15

16

17

18

19

20

21

22

23

24

25

26

27

28 **ABSTRACT**

29 Metabolites and metabolic co-factors can shape the innate immune response, though the
30 pathways by which these molecules adjust inflammation remain incompletely understood. Here
31 we show that the metabolic cofactor Coenzyme A (CoA) enhances IL-4 driven alternative
32 macrophage activation [m(IL-4)] *in vitro* and *in vivo*. Unexpectedly, we found that perturbations in
33 intracellular CoA metabolism did not influence m(IL-4) differentiation. Rather, we discovered that
34 exogenous CoA provides a weak TLR4 signal which primes macrophages for increased
35 receptivity to IL-4 signals and resolution of inflammation via MyD88. Mechanistic studies revealed
36 MyD88-linked signals prime for IL-4 responsiveness, in part, by reshaping chromatin accessibility
37 to enhance transcription of IL-4-linked genes. The results identify CoA as a host metabolic co-
38 factor that influences macrophage function through an extrinsic TLR4-dependent mechanism,
39 and suggests that damage-associated molecular patterns (DAMPs) can prime macrophages for
40 alternative activation and resolution of inflammation.

41

42

43

44

45

46

47

48

49

50

51

52

53

54

55

56

57

58 INTRODUCTION

59 Macrophages are innate immune cells that execute a variety of functions such as detecting
60 and removing foreign pathogens, instructing adaptive immune cell function, secreting cytokines,
61 and maintaining tissue homeostasis. To fulfill these diverse roles, macrophages link the detection
62 of distinct external cues with the engagement of specific transcriptional programs to support
63 different functional states. This process is commonly termed macrophage activation or
64 'polarization'^{1,2}.

65 *In vitro* studies often consider macrophage polarization in two discrete states: classical
66 (Type 1) and alternative (Type 2) activation³. Classical activation is associated with antimicrobial
67 immunity, and occurs when macrophages detect pathogen-associated molecular patterns
68 (PAMPs) such as lipopolysaccharide (LPS) or damage-associated molecular patterns (DAMPs).
69 Alternative activation is associated with wound healing along with allergen and helminth immunity,
70 and is initiated by the macrophage response to interleukin-4 (IL-4) ± IL-13.

71 Along with transcriptional programs that support core macrophage functions such as
72 cytokine secretion and phagocytosis, changes in cellular metabolism are also important and
73 perhaps essential for macrophage effector function⁴⁻⁶. Upon classical activation with LPS,
74 macrophages increase glycolysis and repurpose mitochondria away from oxidative
75 phosphorylation and towards the generation of metabolic signals thought to amplify the pro-
76 inflammatory response⁷⁻¹⁰. Conversely, alternatively activated macrophages (AAMs) display
77 increased rates of oxidative phosphorylation and fatty acid oxidation^{11,12}, though evidence is
78 mixed as to whether these changes are essential for the macrophage IL-4 response [m(IL-4)]¹³⁻
79 ¹⁵. The mechanistic links between how increased oxidative phosphorylation and/or fatty acid
80 oxidation could specifically support m(IL-4) are also unclear. Proposed mechanisms, though,
81 include changes in histone acetylation from enhanced acetyl CoA production¹⁶ as well as
82 transcriptional changes that respond to the mitochondrial membrane potential¹⁷

83 Previous work in our laboratory has associated intracellular levels of CoA with the
84 macrophage IL-4 response^{13,18}. When trying to identify why excess concentrations of the CPT-1
85 inhibitor etomoxir blocked m(IL-4) but genetic ablation of either *Cpt1* or *Cpt2* did not^{14,19}, we
86 discovered that excess etomoxir disrupted macrophage CoA homeostasis. In support of this as a
87 putative mechanism, provision of exogenous CoA restored both intracellular CoA levels as well
88 as the expression of AAM-associated cell surface markers¹³. However, precisely how CoA
89 instructs macrophage activation was not studied.

90 Here we demonstrate that CoA augments AAM function via weak toll-like receptor 4
91 (TLR4) agonism and myeloid differentiation primary response protein 88 (MyD88)-linked

92 signaling, a pathway commonly associated with classical or pro-inflammatory activation. In
93 investigating the mechanism by which exogenous CoA regulates m(IL-4), we surprisingly
94 discovered that CoA provision did not act either by changing intracellular CoA levels or by
95 enhancing known metabolic hallmarks of the IL-4 response. Rather, pharmacologic and genetic
96 approaches showed exogenous CoA is a weak TLR4 agonist and boosts m(IL-4) by activating
97 MyD88-linked signaling. MyD88 agonism was sufficient to enhance *in vitro* and *in vivo* alternative
98 activation and increase chromatin accessibility at the promoter regions of IL-4-target genes. The
99 data show that (i) CoA is a TLR4 agonist, (ii) many of the metabolic hallmarks of the m(IL-4) do
100 not always correlate with anti-inflammatory activation, and (iii) pro-inflammatory MyD88-linked
101 signaling can support AAM function and resolution of inflammation. Furthermore, the results
102 indicate CoA can act as a damage-associated molecular pattern (DAMP) that primes
103 macrophages for the resolution of inflammation by an extrinsic TLR4-dependent mechanism.

104

105 **RESULTS**

106 *Exogenous CoA provision enhances alternative macrophage activation in vitro and in vivo*

107 Prior work had shown that exogenous CoA could rescue the inhibition of m(IL-4) by
108 etomoxir, but the mechanisms underlying this effect were not defined. To better understand how
109 exogenous CoA influenced alternative macrophage activation, mouse bone marrow derived
110 macrophages (BMDMs) were treated with IL-4 alone or in combination with CoA for 48 hr. Gene
111 expression studies revealed that CoA enhanced the expression of multiple IL-4-associated genes,
112 including *Mgl2*, *Pdcd1gl2*, *Fizz1*, *Chil4*, *Ccl8*, *Arg1*, and *Mrc1* (Figure 1a and Supplemental Fig
113 1a)^{17,20-22}. Flow cytometry analysis revealed a similar relationship when measuring IL-4-linked cell
114 surface marker expression. CoA increased the mean fluorescence intensity of CD206 and CD301,
115 as well as the frequency of CD206⁺/CD71⁺ and CD206⁺/CD301⁺ BMDMs (Figs. 1b-d). This effect
116 was observed with CoA concentrations as low as 62.5 μ M (Supplemental Fig. S1b). Importantly,
117 CoA itself did not stimulate the expression of IL-4-associated genes or cell surface markers (Figs.
118 1a-d), demonstrating it is not an IL-4 receptor agonist but rather acts cooperatively to enhance
119 AAM differentiation.

120 Mannose receptor activity is essential for the initiation of the T_H2 response during the
121 helminth infection^{23,24}. Given the observed increase in its gene (*Mrc1*) and protein (CD206)
122 expression, we measured the effect of exogenous CoA on activity of the mannose receptor. As
123 expected, high-content imaging revealed CoA enhanced the cellular uptake of FITC-dextran, a
124 fluorescently labeled polysaccharide and mannose receptor ligand²⁵ (Figs. 1e&f).

125 To assess whether CoA could enhance alternative activation *in vivo*, mice were injected
126 with IL-4 complex (IL-4c) i.p. in the presence or absence of CoA (40 mg/kg). After one day, the
127 peritoneum was flushed and the frequency of CD206⁺/CD71⁺ peritoneal macrophages assessed.
128 Indeed, CoA enhanced the fraction of AAMs co-expressing CD206 and CD71 (Figure 1g),
129 demonstrating that it enhances IL-4-mediated AAM differentiation *in vitro* and *in vivo*.

130

131 CoA does not augment alternative macrophage activation by enhancing metabolic hallmarks of
132 M(IL-4)

133 We next sought to identify the mechanism by which CoA enhances m(IL-4). Several
134 metabolic hallmarks of AAMs require CoA as a necessary cofactor, including enhanced
135 mitochondrial respiratory capacity²⁶⁻²⁸, mitochondrial pyruvate oxidation^{12,29}, and *de novo* lipid
136 synthesis^{30,31}. As such, we hypothesized that addition of exogenous CoA enhanced the IL-4
137 response by increasing intracellular CoA levels to support flux through these metabolic
138 pathways³²⁻³⁴.

139 We first confirmed that exogenously added CoA could expand the cellular CoA pool.
140 Supplementing culture medium with CoA increased the steady-state abundance of both
141 intracellular CoA and acetyl CoA (Fig. 2a). Next, we investigated whether CoA provision
142 enhanced IL-4-driven increases in respiration and glycolysis induced by IL-4^{12,26,30}. Similar to
143 other reports, we observed increases in ATP-linked respiration, maximal respiratory capacity, and
144 glycolysis with IL-4. However, addition of CoA did not further augment these metabolic changes,
145 and even limited the maximal respiratory capacity of AAMs (Figs. 2b-d).

146 After determining that CoA does not enhance alternative macrophage activation via an
147 expansion of bioenergetic capacity, we then examined whether CoA affected other IL-4-linked
148 metabolic alterations such as increased abundance of TCA cycle metabolites²⁹ or enhanced
149 pyruvate oxidation¹², glutamine oxidation²⁹, and *de novo* lipogenesis³¹. Indeed, we reproduced
150 previous reports that show IL-4 increases steady-state levels of select TCA cycle metabolites
151 (Figs. 2e), enrichment from glucose into the TCA cycle (Fig. 2f), and *de novo* lipid synthesis (Fig.
152 2g). However, as before, addition of CoA did not further increase these metabolic changes (Figs.
153 2e-g, S2a-c), and even blocked IL-4-stimulated increases in lipogenesis (Figs. 2g, S2d). As such,
154 the results show exogenous CoA augments alternative activation by a mechanism discrete from
155 reprogramming metabolism.

156

157

158

159 Alterations in intracellular CoA levels are not sufficient to alter M(IL-4)

160 We then questioned whether changes in intracellular CoA levels, in fact, shape the IL-4
161 response. To answer this, we utilized two compounds with opposing impacts on intracellular CoA
162 levels. To decrease steady-state CoA levels, we treated IL-4-stimulated BMDMs with
163 cyclopropane carboxylic acid (CPCA), which decreases the abundance of “free” CoA as its
164 cognate thioester CPC-CoA is formed^{18,35} (Fig. 2h). To increase steady-state CoA levels, we
165 treated IL-4-polarized BMDMs with PZ-2891, a pantothenate kinase agonist which relieves
166 inhibition of CoA biosynthesis³⁶ (Fig. 2h). As expected, CPCA decreased intracellular levels of
167 CoA and acetyl CoA, while PZ-2891 increased their abundance (Fig. 2i, S2e). Surprisingly,
168 despite altering steady-state intracellular CoA levels, neither compound impacted alternative
169 activation (Fig. 2j). The results show that although exogenous CoA provision augments the
170 macrophage IL-4 response, the mechanism cannot be attributed to changing intracellular levels
171 of CoA and acetyl CoA.

172

173 Exogenous CoA induces a macrophage pro-inflammatory response in vitro and in vivo

174 Neither metabolic alterations nor intracellular CoA levels could explain why CoA provision
175 enhanced m(IL-4). Therefore, we sought a more complete understanding of how CoA impacts the
176 transcriptome of AAMs by conducting bulk RNA sequencing (RNA-seq) on naïve macrophages
177 alongside those that were stimulated with either IL-4 or IL-4 with CoA. As expected, cells
178 stimulated only with IL-4 increased the expression of genes associated with alternative activation
179 and decreased expression of genes associated with classical activation relative to vehicle
180 controls. In line with qPCR studies (Fig. 1a), CoA provision further increased the expression of
181 IL-4-linked genes associated with alternative activation (Fig. 3a, *right*). Unexpectedly, however,
182 CoA addition also increased the expression of genes associated with classical activation that
183 were not associated with the IL-4 response (Fig. 3a, *right*). Subsequent Gene Set Enrichment
184 Analysis (GSEA) showed that genes associated with TLR signaling pathways were upregulated
185 upon co-treatment with CoA and IL-4 (Fig. 3b).

186 This unbiased approach suggested that CoA may elicit a pro-inflammatory response in
187 BMDMs along with its ability to enhance m(IL-4). To confirm this, we assessed whether CoA itself
188 could induce expression of pro-inflammatory genes in the absence of IL-4. Indeed, exogenous
189 CoA induced expression of *Il1b*, *Tnf*, *Nos2*, and *Irg1* (Fig. 3c), genes linked to the TLR adaptor
190 protein MyD88, as well as the interferon-stimulated gene (ISG) *Mx1* (Fig. 3d). As *Irg1* encodes
191 the enzyme generating the anti-microbial metabolite itaconate, we also observed a ~10-fold
192 increase in itaconate synthesis upon CoA provision (Fig. 3e). Lastly, i.p. administration of CoA in

193 mice increased expression of *I11b* and *Tnf* in peritoneal leukocytes and increased the abundance
194 of IL-1B, TNF- α , IL-6, and CXCL1 in the peritoneal lavage fluid (Figure 3f&g). Taken together, the
195 results demonstrate that CoA, in addition to enhancing the IL-4 response, elicits a pro-
196 inflammatory response *in vitro* and *in vivo*.

197

198 CoA is a weak TLR4 agonist

199 We then hypothesized that CoA could act as an agonist for a specific TLR. Since the
200 MyD88 adaptor protein is necessary for the full activation of all but one of the murine toll-like
201 receptors³⁷, and CoA stimulated the expression of multiple MyD88-linked pro-inflammatory genes
202 (Fig. 3c), we examined whether the pro-inflammatory response from CoA could persist in BMDMs
203 lacking this signaling adaptor. BMDMs harvested from *Myd88*^{-/-} mice significantly reduced the
204 expression of pro-inflammatory genes induced by CoA, but marginal expression of *I11b*, *Tnfa*, and
205 *Irg1* persisted (Fig. 4a). The result suggested MyD88-dependent and -independent signaling
206 cascades underlie the pro-inflammatory response.

207 We therefore hypothesized that CoA was a TLR4 agonist. Toll-like receptor 4 (TLR4)
208 elicits its inflammatory response by activating both MyD88-dependent and -independent signaling
209 arms³⁸. The MyD88-dependent pathway of TLR4 causes increased expression of cytokines such
210 as *I11b*³⁹, while the TIR-domain-containing adapter-inducing interferon- β (TRIF) pathway is
211 independent of MyD88 and increases expression of ISGs and production of type 1 interferons^{40,41}.
212 Indeed, previous results showed CoA supplementation stimulated expression of the ISG *Mx1*
213 (Fig. 3d).

214 To determine if CoA is a TLR4 agonist, we utilized a reporter cell line which secretes
215 alkaline phosphatase in response to TLR agonism⁴². Addition of CoA activated a cell line
216 expressing human TLR4 (hTLR4) (Fig. 4b, c) but no effect was observed in cells expressing
217 hTLR2 or hTLR7, other Myd88-linked TLRs (Fig. 4c, S3a). Interpolation of an LPS standard curve
218 showed that 1mM CoA had a comparable effect to 0.1ng/mL LPS (Fig. 4b), indicating CoA is a
219 relatively weak TLR4 agonist. BMDMs harvested from *Tlr4*^{-/-} mice further confirmed that CoA acts
220 via TLR4, as CoA did not increase expression of pro-inflammatory genes (Fig. 4d) or production
221 or itaconate (Fig. 4e) in TLR4-deficient macrophages.

222 It was next essential to confirm that the pro-inflammatory response was due to CoA itself
223 rather than an impurity from the >85% pure, yeast-derived CoA used in this study. In support of a
224 direct effect of CoA, cells treated with 99% pure, synthetically-derived CoA elicited a more potent
225 pro-inflammatory response relative to biologically-derived CoA (Fig. S3b,c). Furthermore, both
226 the yeast-derived and synthetically-derived CoA were free of endotoxin as determined by a

227 Limulus test (Fig. S3d). In total, the data demonstrate that CoA directly induces an inflammatory
228 response by acting as a weak TLR4 agonist.

229

230 Myd88-linked TLR agonists enhance the IL-4 response

231 Next, we asked whether TLR4 agonism is the mechanism by which CoA enhances IL-4-
232 mediated alternative activation. Although previous studies have shown that exposure to LPS and
233 interferon gamma (IFN- γ) inhibits the acquisition of m(IL-4)^{26,43}, much of this work has used high
234 concentrations of LPS that correspond to effects that are orders of magnitude greater than that of
235 CoA (calibrated to 0.1 ng/mL; Fig. 4b). We therefore stimulated cells with IL-4 alone or in
236 combination with 0.1ng/mL LPS. Indeed, we observed increased expression of IL-4 dependent
237 cell-surface markers (Figs. 5a&b).

238 To determine which signaling cascade downstream of TLR4 was mediating the enhanced
239 AAM differentiation, we activated macrophages with IL-4 and other TLR ligands that activate
240 either MyD88- or TRIF-dependent signaling. Co-treatment with the MyD88-linked TLR2 agonist
241 Pam3CSK4 (Pam3) increased the population of CD206⁺/CD301⁺ BMDMs, whereas this
242 population was decreased upon co-treatment with the TRIF-linked TLR3 agonist Poly (I:C) (Figs.
243 5a&b). The TLR5 agonist flagellin and the TLR7 agonist imiquimod, both of which are upstream
244 of MyD88, also increased expression of these IL-4-linked cell surface markers, further linking
245 MyD88 with the enhanced m(IL-4). Indeed, LPS (0.1 ng/mL) and Pam3 also increased expression
246 of IL-4-associated genes (Fig. 5c) and mannose receptor activity (Fig. 5d). As with cell surface
247 marker expression, Poly (I:C) co-treatment lowered the expression of IL-4-stimulated genes. To
248 definitively show that MyD88-linked signaling could affect AAM differentiation, we examined
249 whether a low concentration of LPS or Pam3 could enhance the IL-4 response in the absence of
250 MyD88. As expected, the effect of LPS and Pam3 on IL-4-associated cell-surface markers (Fig.
251 5e) and genes (Fig. 5f) was lost in BMDMs isolated from *Myd88*^{-/-} mice.

252 Finally, we determined whether MyD88 agonists could improve M(IL-4) *in vivo* using two
253 independent approaches. First, intraperitoneal injections of either 125 μ g of LPS or 25 μ g Pam3
254 prior to IL-4 complex increased the number of CD206⁺/CD301⁺ cells harvested from the peritoneal
255 cavity, whereas no difference was observed with Poly I:C. (Fig. 5g). As further proof-of-concept,
256 we leveraged a tumor model where alternative macrophage activation supports the growth of
257 implanted B16 melanoma tumors^{15,44}. In line with our previous results, co-treatment of IL-4-
258 stimulated BMDMs with Pam3 resulted in significantly larger tumors when mixed with B16
259 melanoma cells relative to IL-4 alone (Fig. 5h). In combination, these results indicate that
260 activation of the MyD88 pathway enhances alternative macrophage activation *in vitro* and *in vivo*.

261

262 *MyD88 alters the chromatin accessibility of alternatively activated macrophages*

263 Recent studies have highlighted the critical role of epigenetic remodeling when
264 macrophages are exposed to a mix of pro- and anti-inflammatory ligands^{45,46}. We therefore
265 hypothesized that one mechanism by which MyD88 signaling could augment m(IL-4) was by
266 increasing chromatin accessibility in the promoter regions of IL-4 target genes. To test this, we
267 conducted an Assay for Transposase-Accessible Chromatin with high-throughput sequencing
268 (ATAC-seq) analysis on IL-4-stimulated BMDMs with or without co-stimulation with Pam3. We
269 first generated a list of the 10,878 genomic regions which had increased accessibility following
270 IL-4 stimulation [\log_2 fold change (LFC) >1, false discovery rate (FDR) <0.01] relative to vehicle
271 controls. These regions were localized mainly in intergenic and intronic regions (Fig. 6a, S4a).

272 We next assessed whether these IL-4-induced regions had increased accessibility upon
273 co-treatment with Pam3 by creating 10 equal bins in increasing order of LFC values (Fig. 6a,
274 S4b). The analysis revealed over 30% of the IL-4-induced regions were more accessible with
275 TLR2 co-treatment (Bins 8-10; Fig. 6b). To identify potential transcription factors that may mediate
276 the ability of MyD88 to increase alternative activation, we then conducted HOMER transcription
277 factor motif analysis⁴⁷. The analysis indicated that these IL-4-induced regions with increased
278 accessibility following Pam3 co-treatment (Bins 8-10) were enriched for STAT6 and Jun/AP-1
279 binding motifs (Fig. 6b). Moreover, when we expanded our analysis to consider all regions
280 significantly increased by Pam3 (LFC >0.5 and FDR <.05, n = 1766), we noted that these regions
281 were enriched with motifs for the AP-1 subunit *Fra1*, *Stat6* and *Egr2*. (Fig. 6c). Consistent with
282 our hypothesis, the promoter regions of *Chil4* and *Ccl8*, genes we previously associated with the
283 IL-4 response (Fig. 1a), were significantly more accessible upon exposure to Pam3 (Fig. 6d).
284 Additionally, both had significantly more accessible Jun/AP-1 binding motifs following Pam3 co-
285 treatment. Other genes associated with alternative activation such as *Pdcd1g12* and *Arg1* also
286 had consistent, though not statistically significant, increases in accessibility of their promoter
287 regions following Pam3 co-treatment (Fig. S4c). In total, ATAC-Seq analysis shows that MyD88
288 activation regulates chromatin accessibility in AAMs. Further, the data identify the Jun/AP-1 family
289 of transcription factors as candidates that may mediate the synergy between the MyD88 pathway
290 and the IL-4 response.

291

292

293 **DISCUSSION**

294 Our results demonstrate that the ubiquitous metabolic cofactor CoA enhances m(IL-4) in
295 *in vitro* and *in vivo*. Genetic and pharmacologic proof-of-concept studies show, surprisingly, that
296 CoA is a TLR4 agonist and augments alternative activation via MyD88-linked signaling. This
297 discovery and associated data have implications for the metabolic instruction of alternative
298 macrophage activation, the plasticity of macrophage polarization, and the breadth of intracellular
299 metabolites and co-factors that can act as DAMPs.

300 Unexpectedly, addition of exogenous CoA did not augment alternative activation by
301 increasing flux through metabolic pathways linked with m(IL-4). In fact, hallmarks of the IL-4
302 response such as increased respiratory capacity^{17,26,27} and *de novo* lipid synthesis³¹ were
303 significantly reduced by CoA provision. In fact, other work using exogenously added
304 prostaglandins shows AAM markers can further increase beyond what is induced by IL-4 while
305 simultaneously decreasing mitochondrial oxidative metabolism¹⁷. The result suggests there is
306 flexibility in the metabolic phenotypes that can support alternative macrophage activation, and
307 provides an additional data point to the mixed results regarding whether healthy oxidative
308 phosphorylation is obligatory for m(IL-4)^{13,27}.

309 Additionally, gain- and loss-of-function experiments with chemical modulators of
310 intracellular CoA levels revealed that altering CoA levels do not adjust alternative macrophage
311 activation. The rationale for examining this hypothesis arose from studying the effects of the CPT-
312 1 inhibitor etomoxir. High, off-target concentrations of the drug block the macrophage IL-4
313 response and deplete intracellular CoA, and both phenotypes were rescued upon addition of
314 exogenous CoA¹³. The findings presented here, however, show the link between intracellular CoA
315 levels and alternative macrophage activation is likely associative, and suggest the effects of high
316 concentrations of etomoxir are rescued by MyD88-linked signaling rather than restoration of
317 steady-state CoA levels. Although several independent lines of evidence show that etomoxir
318 blocks the IL-4 response via a mechanism independent of fatty acid oxidation^{13-15,48,49} it remains
319 unclear why high concentrations of this lipophilic, reactive epoxide block alternative activation.

320 Various cellular metabolites, including lipids, ATP, and uric acid can function as DAMPs
321 to elicit an *in vitro* pro-inflammatory response⁵⁰⁻⁵². Others, such as the complex lipid prostaglandin
322 E2 and adenosine, can enhance alternative activation^{17,53}. Here we show that CoA is a putative
323 DAMP that primes macrophages for alternative activation and supports resolution via extrinsic,
324 weak agonism of pro-inflammatory TLR4 and MyD88 signaling.

325 This aligns with recent reports that show CoA increases the expression of pro-
326 inflammatory genes such as *Il1b*, *Tnf* and *Nos2* in mouse and human macrophages, an effect
327 lost in mice with simultaneous genetic ablation of TLR2, TLR4, and the TLR chaperone protein

328 Uncb93b1⁵⁴. The data presented here that CoA itself is a TLR4 agonist likely explains the effect,
329 rather than CoA having an indirect effect on the pro-inflammatory response via altered
330 mitochondrial metabolism. As CoA consists of an adenosine diphosphate group linked to a
331 phosphopantetheine moiety³², CoA is chemically distinct from many well characterized TLR4
332 agonists⁵⁵. Interestingly, nucleoside analogues such as imiquimod (a guanosine analogue) and
333 CL264 (an adenine analogue) are potent TLR7/8 agonists. However, CoA did not activate hTLR7
334 reporter cells, and additional work is required to understand the structural specificity that enables
335 CoA to specifically activate TLR4.

336 TLR4 is well characterized for its ability to respond to ligands that are derived from
337 microbes, and its role in sensing endogenous ligands is increasingly appreciated⁵⁶. Release of
338 intracellular proteins including tenascin 1 and high-mobility group box 1 (HMGB1) can induce a
339 TLR4-dependent inflammatory response^{42,57,58}, but the capacity for intracellular metabolites and
340 metabolic co-factors to activate TLR4 is less established⁵⁹. Here we show with genetic and
341 pharmacologic proof-of-concept studies that CoA is an endogenous metabolic co-factor that can
342 extrinsically activate TLR4 at physiologically relevant concentrations. Intracellular CoA
343 concentrations can reach over 100 μ M in the cytosol and up to 5 mM in the mitochondrial
344 matrix^{32,34,60}. As such, cell injury or death could release sufficient CoA to trigger a TLR4-mediated
345 inflammatory response in nearby innate immune cells, particularly in regions where DAMPs can
346 accumulate such as poorly vascularized areas. Other intracellular metabolites function as DAMPs
347 following their cell death-induced release^{61,62}, and given that CoA contains an ADP moiety, the
348 findings are broadly consistent with the finding that adenosine can enhance the macrophage IL-
349 4 response via the A2 adenosine receptor⁵³.

350 Although macrophage polarization is often bifurcated into classical or alternative
351 activation, the physiological and pathological induction of an innate immune response involves
352 heterogeneity in activation signals and functional state^{3,63,64}. For example, healing processes such
353 as muscle and skin repair are characterized by both an initial influx of pro-inflammatory
354 macrophages to stem infection, as well as a subsequent increase in the presence of alternatively
355 activated macrophages to promote resolution and tissue repair^{65,66}. This plasticity can be
356 important for proper function. For example, inhibition of the initial pro-inflammatory response
357 dampens the future expression of alternative activation markers and decreases wound healing⁶⁷.

358 Cooperativity between classical and alternative macrophage activation has been
359 established for more than 20 years, with studies demonstrating that IL-4 can enhance the
360 expression of LPS-induced pro-inflammatory genes⁶⁸. Recent studies have corroborated these
361 findings by demonstrating that IL-4 epigenetically primes macrophages to enhance the

362 transcriptional response to pro-inflammatory stimuli⁴⁶. Indeed, our work suggests that pro-
363 inflammatory MyD88-linked signaling enhances the IL-4 response, at least in part, by altering
364 chromatin accessibility.

365 Recent work provides strong support that MyD88-linked signaling via TLR4 agonism is a
366 plausible mechanism by which CoA can augment m(IL-4)⁶⁹⁻⁷². For example, the fungal effector
367 protein CLP-1, a TLR4 agonist, fails to enhance alternative activation in MyD88^{-/-} BMDMs.
368 Moreover, other work has associated AAMs with IL-33⁷³, which is upstream of MyD88. Others
369 have also shown that interferon- β decreases the expression of cell surface markers and genes
370 associated with alternative activation^{45,74,75}, further supporting our findings that TLR4 agonism by
371 CoA enhances m(IL-4) via MyD88 rather than TRIF. The ATAC-Seq analysis presented here
372 furthers this work by identifying Jun/AP-1 signaling as a candidate pathway downstream of MyD88
373 that may mediate the enhanced IL-4 response.

374

375 **MATERIALS AND METHODS**

376 Animals

377 All animal protocols and procedures were approved and performed in accordance with the
378 NIH Guide for the Care and Use of Laboratory Animals and the UCLA Animal Research
379 Committee (ARC).

380

381 Reagents

382 Unless otherwise specified, yeast-derived CoA that was purchased from Sigma-Aldrich
383 (C4780; $\geq 85\%$ purity) was used. Synthetic CoA was purchased from Avanti Polar Lipids
384 (870700P; $>99\%$ purity). IL-4 was purchased from PeproTech (214-14), and IL-4-reactive
385 monoclonal antibodies for *in vivo* studies (IL-4 MAb) were purchased from BioXCell (BE0045). All
386 TLR agonists were purchased from Invivogen: Pam3CSK4 (TLR2 ligand; tlr1-pms), Poly(I:C)
387 (TLR3 ligand; tlr1-pic), LPS (TLR4 ligand; tlr1-smlps), Flagellin (TLR5 ligand; tlr1-stfla), and
388 imiquimod (TLR7 agonist; tlr1-imqs-1).

389

390 Isolation and differentiation of mouse BMDMs

391 BMDMs from wild-type (000664), Myd88^{-/-} (009088), and Tlr4^{-/-} (029015) mice were
392 isolated as previously described from male mice aged between 6-12 weeks⁷⁶. Briefly, bone
393 marrow cells were first isolated by flushing the femurs and tibiae with phosphate buffered saline
394 (PBS). Cells were then pelleted by centrifugation at 365g for 7 mins at room temperature.

395 Following the removal of red blood cells with RBC Lysis Buffer (Sigma, R7757) and centrifugation,
396 bone marrow cells were differentiated for 6 days at 37°C in a humidified 5% CO₂ incubator in
397 'BMDM differentiation medium'. BMDM differentiation medium consisted of DMEM (Gibco
398 #11965) supplemented with 10% (v/v) fetal bovine serum (FBS; Hyclone), 2mM L-glutamine,
399 500µM sodium pyruvate, 100 units/mL, 100 mg/mL penicillin/streptomycin,. Additionally, the
400 medium was further supplemented 10% (v/v) with the conditioned medium from CMG-14-12 cells
401 as a source of macrophage colony stimulate factor (M-CSF).

402

403 *In vitro BMDM activation and stimulation of Toll-like receptors*

404 After six days of differentiation, BMDMs were scraped with a cell lifter, counted, and
405 replated at the listed cell densities into the relevant assay format (e.g., six-well tissue culture dish,
406 Seahorse XF96-well plate, etc.) in differentiation medium. After two days, cells were stimulated
407 with compounds as indicated below and in the figure legends. Unless otherwise specified, all
408 measurements of the macrophage IL-4 response were conducted 48 hr. after treatment. When
409 assessing the effect of CoA on the pro-inflammatory response, BMDMs were treated for 4 hr.
410 (gene expression) or 24 hr. (itaconate abundance). Unless otherwise indicated in the figures and
411 legends, effector compounds were used at the following concentrations alongside matched
412 vehicle controls: IL-4 (20 ng/mL), CoA (1 mM), Pam3CSK4 (5 ng/mL), Poly(I:C) (1µg/mL), LPS
413 (0.1 ng/mL), flagellin (100ng/mL), and imiquimod (10µM).

414

415 *In vivo activation of peritoneal macrophages*

416 To induce alternative activation *in vivo*, mice were treated with an IL-4 complex (IL-4c)
417 consisting of a 2:1 molar ratio of IL-4 and anti-IL-4 mAb or PBS as a control. Each IL-4c-treated
418 mouse received 5µg IL-4 and 25µg of anti-IL-4 mAb. To test the effect of CoA on alternative
419 activation *in vivo* (Fig. 1g), mice were pretreated with an injection of either PBS or 40 mg/kg CoA
420 for 6 hr. prior to IL-4c administration according to the scheme in the figure. After 24 hr. peritoneal
421 macrophages were collected by rinsing the peritoneal cavity with 5mL PBS, and alternative
422 activation markers were assessed using flow cytometry.

423 To determine if CoA could induce a pro-inflammatory response *in vivo* (Figs. 3f&g), mice
424 were treated with either PBS or 40 mg/kg CoA for 6 hr. After treatment, peritoneal macrophages
425 were collected by rinsing the peritoneal cavity with 5mL of PBS. Cells were then pelleted, with
426 supernatant used to measure cytokine levels with the LEGENDplex multiplex ELISA kit
427 (Biolegend, 740848), while gene expression was measured in the peritoneal exudate cells..

428 To determine if TLR agonists could enhance the IL-4 response of peritoneal macrophages
429 *in vivo* (Fig. 5g), Mice were treated with either PBS or the indicated TLR agonist at the following
430 doses: Pam3CSK4 (50µg), Poly:IC (200µg), or LPS (125µg). After 24 hr. IL-4c was administered
431 as before, and the number of cells double-positive for CD206 and CD301 was assessed by flow
432 cytometry.

433

434 *B16 melanoma growth*

435 Prior to *in vivo* co-injection, *in vitro* BMDMs were either stimulated with vehicle control, IL-4 , or
436 IL-4 in combination with Pam3CSK4 for 48 hrs. On the day of implantation, a 1:1 mixture of
437 1×10^5 B16-F10 cells and 1×10^5 BMDMs were suspended in PBS and injected into the rear right
438 flanks of 12 week old Male C57BL/6 mice¹⁵. Mice were sacrificed 20 days post injection and
439 subcutaneous tumors were excised, blotted dry, and weighed.

440

441 *Gene expression analysis*

442 Gene transcript levels were measured using qPCR. On Day 6 of differentiation, BMDMs
443 were seeded at 3.0×10^5 cells/well in 12-well plates. After activating cells with the concentrations
444 and durations as described earlier, RNA was extracted using the RNeasy Mini Kit (Qiagen, 74106)
445 and cDNA was synthesized using high-capacity cDNA reverse transcription kit (Applied
446 Biosystems, 4368814) according to the manufacturers' protocol. qPCR was performed with
447 PowerUp SYBR green master mix (Applied Biosystems, A25743) on a QuantStudio 5 RT-PCR
448 (Applied Biosystems). Relative gene expression values were calculated using the delta-delta Ct
449 method, with the ribosomal protein *Rplp0* used as a control for normalization.

450

451 *Flow cytometric analysis*

452 Cell surface marker expression was measured using flow cytometry. On Day 6 of
453 differentiation, BMDMs were seeded at 3.0×10^5 cells/well in 12-well plates. After activating cells
454 with the concentrations and durations as described earlier, BMDMs were detached by scraping
455 in 450µL of Accutase. Cells were then washed with FACS buffer (PBS+ 2% (v/v) FBS with 1mM
456 EDTA) and incubated with a 1:500 dilution of TruStain FCX (Biolegend, 101320) for 5 minutes.
457 Cells were next stained for 30 mins on ice with a 1:300 dilution of antibodies raised against mouse
458 CD206 (Biolegend,141710), CD301(Biorad, MCA2392A647T), or CD71(Biolegend, 113812).
459 Cells were then washed and resuspended in FACS buffer containing 1 µg/mL DAPI (Invitrogen,
460 D1306) for viability analysis, and data was captured on an Attune NXT flow cytometer. Data were
461 analyzed using FlowJo X software.

462 Endocytosis assay

463 Following differentiation, BMDMs were seeded in black-walled 96-well plates at 3×10^4
464 cells/well for high-content imaging to quantify uptake of FITC-dextran. 48 hr. after compound
465 treatment, medium was replaced with high-glucose DMEM containing 1mg/mL FITC-dextran
466 (Sigma, FD40) and 10ng/mL Hoechst 33342. Following a 1hr. incubation at 37°C, cells were
467 washed twice with PBS and fixed with 4% (v/v) paraformaldehyde (PFA) in PBS. Images were
468 captured with a PerkinElmer Operetta, and FITC-positive foci per cell was calculated using
469 Harmony software.

470

471 Quantification of short-chain acyl CoAs

472 Quantification of acyl CoAs was conducted according to previously established methods¹⁸
473 . Following differentiation, BMDMs were seeded in 10cm² dishes at 5×10^6 cells/dish. Following
474 48hr. stimulation, cells were rinsed twice with ice-cold PBS, scraped into 1.5mL microfuge tubes
475 and pelleted via centrifugation at 4°C . 200µL of an ice-cold extraction solution [2.5% (w/v) 5-
476 sulfosalicylic acid (SSA) along with 1µM Crotonoyl CoA as an internal standard] was added to
477 each cell pellet and subsequently vortexed. Samples were centrifuged at 18,000g for 15 min at
478 4°C. Supernatants containing short-chain acyl CoAs were then removed and transferred to glass
479 LC-MS vials for analysis as is thoroughly described elsewhere¹⁸ .

480

481 Seahorse XF Analysis

482 After 6 days of differentiation, BMDMs were plated at 3.0×10^4 cells/well in XF96 plates.
483 Following 48 hr. of treatment with compounds under investigation, respirometry assays were
484 conducted with an Agilent Seahorse XFe96 Analyzer. Oligomycin (2 µM), two injections of FCCP
485 (750 nM each), and rotenone (200 nM) with antimycin A (1 µM) were added acutely to the wells,
486 and respiratory parameters calculated according to best practices^{77,78}. Measurements were
487 conducted in unbuffered DMEM (Sigma #5030) supplemented with 5 mM HEPES, 8 mM glucose,
488 2 mM glutamine, and 2 mM pyruvate. Lactate efflux was measured by correcting rates of
489 extracellular acidification for microplate sensor coverage and confounding respiratory
490 acidification⁷⁹.

491 Metabolomics and stable isotope tracing of polar metabolites

492 After 6 days of differentiation, BMDMs were plated at 1×10^6 cells/well in 6-well dishes.
493 Cells were then stimulated in medium where either glucose or glutamine was replaced with
494 uniformly labeled ¹³C₆-glucose (CLM-1396) or uniformly labeled ¹³C₅-glutamine (CLM-1822). After
495 48 hr., cells were harvested and extracted for GC/MS using established methods, with all steps

496 conducted on ice⁸⁰. Briefly, cell plates were washed twice with 0.9% (w/v) NaCl and samples were
497 extracted with 500 μ L methanol, 200 μ L water containing 1 μ g of norvaline (internal standard),
498 and 500 μ L chloroform. Samples were vortexed for 1 min and spun at 10,000 g for 5 min at 4°C,
499 and the aqueous layers containing the polar metabolites were transferred to GC/MS sample vials
500 and dried overnight using a refrigerated CentriVap. Once dry, the samples were resuspended in
501 20 μ L of 2% (w/v) methoxyamine in pyridine and incubated at 37°C for 45 minutes. This was
502 followed by addition of 20 μ L of MTBSTFA + 1% TBDMS (N-tert-Butyldimethylsilyl-N-
503 methyltrifluoroacetamide with 1% tertButyldimethylchlorosilane). Following a second 45-minute
504 incubation at 37°C, samples were run as previously described⁸⁰. Analysis was conducted using
505 Agilent MassHunter software, and stable isotope tracing data was corrected for natural
506 abundance of heavy isotopes with FluxFix software using a reference set of unlabeled metabolite
507 standards⁸¹.

508

509 *De novo lipogenesis*

510 Briefly, after 6 days of differentiation, BMDMs were plated at 1×10^5 cells/ well in 24-well
511 dishes Cells were stimulated in medium in which unlabeled glucose was replaced with 10mM
512 uniformly labeled ¹³C₆-glucose. Extraction of fatty acids, quantification of *de novo* synthesis, and
513 normalization to cell number was conducted using an Agilent 5975C mass spectrometer coupled
514 to a 7890 gas chromatograph as previously described^{76,82}.

515

516 *HEK-Blue hTLR reporter assays*

517 HEK-Blue reporter cells expressing either human TLR2 (hkb-htlr2), hTLR4 (hkb-htlr4), or
518 hTLR7 (hkb-htlr7v2) were purchased from InvivoGen and maintained according to the
519 manufacturer's instructions. To establish concentration-response curves, 2.5×10^3 reporter cells
520 were resuspended in HEK-Blue detection medium (Invivogen, hb-det2) in 96-well plates and
521 stimulated with the appropriate agonist (Pam3CSK4: 0.6pg/mL to 1 μ g/mL; LPS: 0.6pg/mL to 1
522 μ g/mL; CL307: 0.6pg/mL to 1 μ g/mL). Following a 24hr. incubation, secreted alkaline
523 phosphatase reporter activity was determined by assessing OD₆₃₀ with a plate reader. The OD₆₃₀
524 of cells treated with 1 mM CoA was compared relative to positive controls. Calibration cuves to
525 fit empirical data were generated using GraphPad Prism software.

526

527

528

529 ATAC-Seq library prep

530 ATAC-seq libraries were produced by the Applied Genomics, Computation and Translational Core
531 Facility at Cedars Sinai. Briefly 50,000 BMDMs per sample were lysed to collect nuclei and treated
532 with Tn5 transposase (Illumina) for 30 min at 37°C with gentle agitation. The DNA was isolated
533 with DNA Clean & Concentrator Kit (Zymo) and PCR amplified and barcoded with NEBNext High-
534 Fidelity PCR Mix (New England Biolabs) and unique dual indexes (Illumina). The ATAC-seq
535 library amplification was confirmed by real-time PCR, and additional barcoding PCR cycles were
536 added as necessary while avoiding overamplification. Amplified ATAC-seq libraries were purified
537 with DNA Clean & Concentrator Kit (Zymo). The purified libraries were quantified with Kapa
538 Library Quant Kit (KAPA Biosystems) and quality assessed on a 4200 TapeStation System
539 (Agilent). The libraries were pooled based on molar concentrations and sequenced on a HiSeq
540 4000 platform (paired end, 100 bp).

541

542 ATAC-Seq analysis

543 The peaks for all the ATAC-seq samples were used to generate a single reference peak file, and
544 the number of reads that fell into each peak was counted using deeptools multiBamSummary⁸³.
545 EdgeR⁸⁴ was used to determine the IL-4 significantly induced regions by applying a cutoff FDR
546 <0.01 and LFC > 1 of triplicate data upon IL-4 stimulation on WT BMDMs and to determine the
547 Pam3CSK4 co-treatment significant regions by applying a cutoff FDR <0.05 and LFC > 0.5.
548 Analysis of transcription factor motif enrichment was performed using findMotifsGenome function
549 in the HOMER suite⁴⁷, using all detected peaks as background. Reads were normalized by RPKM.
550 Data were visualized with ggplot2 or the pheatmap packages in R.

551

552 RNA-Seq library prep and quantification

553 RNA sequencing libraries were produced by the Technology Center for Genomics &
554 Bioinformatics at UCLA. Isolation of RNA was performed using Qiagen RNeasy Mini kit and RNA
555 libraries were prepared with KAPA stranded mRNA-Seq kit. High throughput sequencing was
556 performed on Illumina NovaSeq 6000 (paired end, 2x150bp) targeting 100 million reads per
557 sample. Demultiplexing was performed with Illumina Bcl2fastq v2.19.1. Gene expression
558 quantification from the resulting fastqs was performed using Salmon v1.21.1 in mapping-based
559 mode (Patro et al. 2017). Reads were selectively aligned to the GENCODE vM25 mouse
560 reference transcriptome with corrections for sequence-specific and GC content biases.

561

562 RNA-Seq analysis

563 Raw gene count data were analyzed using the R package DESeq2 v1.22.2⁸⁵ for library size
564 normalization and differential expression analysis. For differential expression results, genes with
565 adjusted p-values below 0.01 and log2 fold changes above 1 or below -1 were deemed significant.
566 For visualization in volcano plots, log2 fold changes above 10 or below -10 were set to 10 and -
567 10 respectively. Gene set enrichment analysis⁸⁶ was performed using the R package FGSEA
568 v1.15.0⁸⁷ based on gene lists ranked by the Wald statistic from differential expression results.
569 Genesets corresponding to the mouse transcriptome from KEGG, REACTOME, and BIOCARTA
570 within the Molecular Signatures Database⁸⁸ were accessed using the R package msigdb v7.1.1⁸⁹
571 Genesets with adjusted p-values below 0.05 were deemed significant.

572

573 Statistical analysis

574 All statistical parameters, including the number of biological replicates (n), can be found
575 in the figure legends. Statistical analyses were performed using Graph Pad Prism 5 software.
576 Data are presented as the mean \pm standard deviation unless otherwise specified. Individual
577 pairwise comparisons were performed using two-tailed Student's t-test. For analysis involving
578 more than two groups, data were analyzed by repeated measures ANOVA followed by Dunnett's
579 post-hoc multiple comparisons tests (compared against vehicle controls unless otherwise
580 specified). Data were assumed to follow a normal distribution (no tests were performed). Values
581 denoted as follows were considered statistically significant: *, $p < 0.05$; **, $p < 0.01$; ***, $p < 0.001$.
582

583 **AUTHOR CONTRIBUTIONS**

584 Conceptualization: AEJ, SJB, ASD; Data curation: AEJ, AR, NI, CC, NAB, ASD; Formal analysis:
585 AEJ, AR, NI, CC, NAB, ASD; Funding acquisition: TGG, AH, SJB, ASD; Investigation: AEJ, AR,
586 NI, CC, NAB, ABB, WYH, AS, ARB, AAC; Methodology: AEJ, CC, NAB, AS, ASD; Project
587 administration: SJB, ASD; Resources: TGG, AH, SJB, ASD; Supervision: AEJ, SJB, ASD ; Writing
588 - original draft: AEJ, ASD; Writing - review & editing: All authors
589

590 **ACKNOWLEDGEMENTS**

591 ASD is supported by National Institutes of Health (NIH) Grant R35GM138003, the W.M. Keck
592 Foundation (995337), and the Agilent Early Career Professor Award. SJB is supported by the NIH
593 Grants P01HL146358 and R01HL157710. AEJ was supported by the UCLA Tumor Cell Biology
594 Training Program T32 CA009056. ABB is supported by the UCLA Chemistry-Biology Interface
595 Training Grant T32GM136614. AH is supported by NIH Grant R01AI173214.

596

597 DISCLOSURES

598 None

599

600 REFERENCES

- 601 1 Glass, C. K. & Natoli, G. Molecular control of activation and priming in macrophages. *Nat*
602 *Immunol* **17**, 26-33, doi:10.1038/ni.3306 (2016).
- 603 2 Murray, P. J. Macrophage Polarization. *Annu Rev Physiol* **79**, 541-566,
604 doi:10.1146/annurev-physiol-022516-034339 (2017).
- 605 3 Murray, P. J. *et al.* Macrophage activation and polarization: nomenclature and
606 experimental guidelines. *Immunity* **41**, 14-20, doi:10.1016/j.immuni.2014.06.008 (2014).
- 607 4 Van den Bossche, J., O'Neill, L. A. & Menon, D. Macrophage Immunometabolism: Where
608 Are We (Going)? *Trends Immunol* **38**, 395-406, doi:10.1016/j.it.2017.03.001 (2017).
- 609 5 Jones, A. E. & Divakaruni, A. S. Macrophage activation as an archetype of mitochondrial
610 repurposing. *Mol Aspects Med* **71**, 100838, doi:10.1016/j.mam.2019.100838 (2020).
- 611 6 Wculek, S. K., Dunphy, G., Heras-Murillo, I., Mastrangelo, A. & Sancho, D. Metabolism of
612 tissue macrophages in homeostasis and pathology. *Cell Mol Immunol* **19**, 384-408,
613 doi:10.1038/s41423-021-00791-9 (2022).
- 614 7 Tannahill, G. M. *et al.* Succinate is an inflammatory signal that induces IL-1 β through HIF-
615 1 α . *Nature* **496**, 238-242, doi:10.1038/nature11986 (2013).
- 616 8 Haschemi, A. *et al.* The sedoheptulose kinase CARKL directs macrophage polarization
617 through control of glucose metabolism. *Cell Metab* **15**, 813-826,
618 doi:10.1016/j.cmet.2012.04.023 (2012).
- 619 9 Mills, E. L. *et al.* Succinate Dehydrogenase Supports Metabolic Repurposing of
620 Mitochondria to Drive Inflammatory Macrophages. *Cell* **167**, 457-470.e413,
621 doi:10.1016/j.cell.2016.08.064 (2016).
- 622 10 Britt, E. C. *et al.* Switching to the cyclic pentose phosphate pathway powers the oxidative
623 burst in activated neutrophils. *Nat Metab* **4**, 389-403, doi:10.1038/s42255-022-00550-8
624 (2022).
- 625 11 Vats, D. *et al.* Oxidative metabolism and PGC-1 β attenuate macrophage-mediated
626 inflammation. *Cell Metab* **4**, 13-24, doi:10.1016/j.cmet.2006.05.011 (2006).
- 627 12 Huang, S. C. *et al.* Metabolic Reprogramming Mediated by the mTORC2-IRF4 Signaling
628 Axis Is Essential for Macrophage Alternative Activation. *Immunity* **45**, 817-830,
629 doi:10.1016/j.immuni.2016.09.016 (2016).
- 630 13 Divakaruni, A. S. *et al.* Etomoxir Inhibits Macrophage Polarization by Disrupting CoA
631 Homeostasis. *Cell Metab* **28**, 490-503.e497, doi:10.1016/j.cmet.2018.06.001 (2018).
- 632 14 Van den Bossche, J. & van der Windt, G. J. W. Fatty Acid Oxidation in Macrophages and
633 T Cells: Time for Reassessment? *Cell Metab* **28**, 538-540,
634 doi:10.1016/j.cmet.2018.09.018 (2018).
- 635 15 Bakker, N. v. T. *et al.* In macrophages fatty acid oxidation spares glutamate for use in
636 diverse metabolic pathways required for alternative activation. *bioRxiv*,
637 2022.2004.2013.487890, doi:10.1101/2022.04.13.487890 (2022).
- 638 16 Covarrubias, A. J. *et al.* Akt-mTORC1 signaling regulates Acly to integrate metabolic input
639 to control of macrophage activation. *Elife* **5**, doi:10.7554/eLife.11612 (2016).
- 640 17 Sanin, D. E. *et al.* Mitochondrial Membrane Potential Regulates Nuclear Gene Expression
641 in Macrophages Exposed to Prostaglandin E2. *Immunity* **49**, 1021-1033.e1026,
642 doi:10.1016/j.immuni.2018.10.011 (2018).

- 643 18 Jones, A. E. *et al.* A Single LC-MS/MS Analysis to Quantify CoA Biosynthetic
644 Intermediates and Short-Chain Acyl CoAs. *Metabolites* **11**, doi:10.3390/metabo11080468
645 (2021).
- 646 19 Gonzalez-Hurtado, E. *et al.* Loss of macrophage fatty acid oxidation does not potentiate
647 systemic metabolic dysfunction. *Am J Physiol Endocrinol Metab* **312**, E381-e393,
648 doi:10.1152/ajpendo.00408.2016 (2017).
- 649 20 Liu, P. S. *et al.* α -ketoglutarate orchestrates macrophage activation through metabolic and
650 epigenetic reprogramming. *Nat Immunol* **18**, 985-994, doi:10.1038/ni.3796 (2017).
- 651 21 Zhang, X. *et al.* CCL8 secreted by tumor-associated macrophages promotes invasion and
652 stemness of glioblastoma cells via ERK1/2 signaling. *Lab Invest* **100**, 619-629,
653 doi:10.1038/s41374-019-0345-3 (2020).
- 654 22 Webb, D. C., McKenzie, A. N. & Foster, P. S. Expression of the Ym2 lectin-binding protein
655 is dependent on interleukin (IL)-4 and IL-13 signal transduction: identification of a novel
656 allergy-associated protein. *J Biol Chem* **276**, 41969-41976, doi:10.1074/jbc.M106223200
657 (2001).
- 658 23 van Die, I. & Cummings, R. D. The Mannose Receptor in Regulation of Helminth-Mediated
659 Host Immunity. *Front Immunol* **8**, 1677, doi:10.3389/fimmu.2017.01677 (2017).
- 660 24 van Liempt, E. *et al.* Schistosoma mansoni soluble egg antigens are internalized by human
661 dendritic cells through multiple C-type lectins and suppress TLR-induced dendritic cell
662 activation. *Mol Immunol* **44**, 2605-2615, doi:10.1016/j.molimm.2006.12.012 (2007).
- 663 25 Sallusto, F., Cella, M., Danieli, C. & Lanzavecchia, A. Dendritic cells use macropinocytosis
664 and the mannose receptor to concentrate macromolecules in the major histocompatibility
665 complex class II compartment: downregulation by cytokines and bacterial products. *J Exp*
666 *Med* **182**, 389-400, doi:10.1084/jem.182.2.389 (1995).
- 667 26 Van den Bossche, J. *et al.* Mitochondrial Dysfunction Prevents Repolarization of
668 Inflammatory Macrophages. *Cell Rep* **17**, 684-696, doi:10.1016/j.celrep.2016.09.008
669 (2016).
- 670 27 Puleston, D. J. *et al.* Polyamines and eIF5A Hypusination Modulate Mitochondrial
671 Respiration and Macrophage Activation. *Cell Metab* **30**, 352-363.e358,
672 doi:10.1016/j.cmet.2019.05.003 (2019).
- 673 28 Tan, Z. *et al.* Pyruvate Dehydrogenase Kinase 1 Participates in Macrophage Polarization
674 via Regulating Glucose Metabolism. *The Journal of Immunology* **194**, 6082-6089,
675 doi:10.4049/jimmunol.1402469 (2015).
- 676 29 Jha, A. K. *et al.* Network integration of parallel metabolic and transcriptional data reveals
677 metabolic modules that regulate macrophage polarization. *Immunity* **42**, 419-430,
678 doi:10.1016/j.immuni.2015.02.005 (2015).
- 679 30 Huang, S. C. *et al.* Cell-intrinsic lysosomal lipolysis is essential for alternative activation of
680 macrophages. *Nat Immunol* **15**, 846-855, doi:10.1038/ni.2956 (2014).
- 681 31 Bidault, G. *et al.* SREBP1-induced fatty acid synthesis depletes macrophages antioxidant
682 defences to promote their alternative activation. *Nat Metab* **3**, 1150-1162,
683 doi:10.1038/s42255-021-00440-5 (2021).
- 684 32 Leonardi, R., Zhang, Y. M., Rock, C. O. & Jackowski, S. Coenzyme A: back in action. *Prog*
685 *Lipid Res* **44**, 125-153, doi:10.1016/j.plipres.2005.04.001 (2005).
- 686 33 Pietrocola, F., Galluzzi, L., Bravo-San Pedro, J. M., Madeo, F. & Kroemer, G. Acetyl
687 coenzyme A: a central metabolite and second messenger. *Cell Metab* **21**, 805-821,
688 doi:10.1016/j.cmet.2015.05.014 (2015).
- 689 34 Gout, I. Coenzyme A, protein CoAlation and redox regulation in mammalian cells.
690 *Biochem Soc Trans* **46**, 721-728, doi:10.1042/bst20170506 (2018).
- 691 35 Steinhilber, M. E. & Olson, M. S. The effects of cyclopropane carboxylate on hepatic
692 pyruvate metabolism. *Arch Biochem Biophys* **243**, 80-91, doi:10.1016/0003-
693 9861(85)90775-1 (1985).

- 694 36 Sharma, L. K. *et al.* A therapeutic approach to pantothenate kinase associated
695 neurodegeneration. *Nature Communications* **9**, 4399, doi:10.1038/s41467-018-06703-2
696 (2018).
- 697 37 Snyder, G. A. *et al.* Molecular mechanisms for the subversion of MyD88 signaling by TcpC
698 from virulent uropathogenic *Escherichia coli*. *Proceedings of the National Academy*
699 *of Sciences* **110**, 6985-6990, doi:10.1073/pnas.1215770110 (2013).
- 700 38 Fitzgerald, K. A. & Kagan, J. C. Toll-like Receptors and the Control of Immunity. *Cell* **180**,
701 1044-1066, doi:10.1016/j.cell.2020.02.041 (2020).
- 702 39 Kawai, T., Adachi, O., Ogawa, T., Takeda, K. & Akira, S. Unresponsiveness of MyD88-
703 deficient mice to endotoxin. *Immunity* **11**, 115-122, doi:10.1016/s1074-7613(00)80086-2
704 (1999).
- 705 40 Kawai, T. *et al.* Lipopolysaccharide stimulates the MyD88-independent pathway and
706 results in activation of IFN-regulatory factor 3 and the expression of a subset of
707 lipopolysaccharide-inducible genes. *J Immunol* **167**, 5887-5894,
708 doi:10.4049/jimmunol.167.10.5887 (2001).
- 709 41 Toshchakov, V. *et al.* TLR4, but not TLR2, mediates IFN-beta-induced STAT1alpha/beta-
710 dependent gene expression in macrophages. *Nat Immunol* **3**, 392-398, doi:10.1038/ni774
711 (2002).
- 712 42 Sosa, R. A. *et al.* Disulfide High-Mobility Group Box 1 Drives Ischemia-Reperfusion Injury
713 in Human Liver Transplantation. *Hepatology* **73**, 1158-1175, doi:10.1002/hep.31324
714 (2021).
- 715 43 Khallou-Laschet, J. *et al.* Macrophage Plasticity in Experimental Atherosclerosis. *PLOS*
716 *ONE* **5**, e8852, doi:10.1371/journal.pone.0008852 (2010).
- 717 44 Chen, X. W. *et al.* CYP4A in tumor-associated macrophages promotes pre-metastatic
718 niche formation and metastasis. *Oncogene* **36**, 5045-5057, doi:10.1038/onc.2017.118
719 (2017).
- 720 45 Dichtl, S. *et al.* Gene-selective transcription promotes the inhibition of tissue reparative
721 macrophages by TNF. *Life Sci Alliance* **5**, doi:10.26508/lsa.202101315 (2022).
- 722 46 Czimmerer, Z. *et al.* The epigenetic state of IL-4-polarized macrophages enables
723 inflammatory cistromic expansion and extended synergistic response to TLR ligands.
724 *Immunity* **55**, 2006-2026.e2006, doi:10.1016/j.immuni.2022.10.004 (2022).
- 725 47 Heinz, S. *et al.* Simple combinations of lineage-determining transcription factors prime cis-
726 regulatory elements required for macrophage and B cell identities. *Mol Cell* **38**, 576-589,
727 doi:10.1016/j.molcel.2010.05.004 (2010).
- 728 48 Ceccarelli, S. M., Chomienne, O., Gubler, M. & Arduini, A. Carnitine palmitoyltransferase
729 (CPT) modulators: a medicinal chemistry perspective on 35 years of research. *J Med*
730 *Chem* **54**, 3109-3152, doi:10.1021/jm100809g (2011).
- 731 49 Nomura, M. *et al.* Fatty acid oxidation in macrophage polarization. *Nat Immunol* **17**, 216-
732 217, doi:10.1038/ni.3366 (2016).
- 733 50 Kim, S. M. *et al.* Hyperuricemia-induced NLRP3 activation of macrophages contributes to
734 the progression of diabetic nephropathy. *Am J Physiol Renal Physiol* **308**, F993-f1003,
735 doi:10.1152/ajprenal.00637.2014 (2015).
- 736 51 Wang, X., Wang, Y., Antony, V., Sun, H. & Liang, G. Metabolism-Associated Molecular
737 Patterns (MAMPs). *Trends Endocrinol Metab* **31**, 712-724, doi:10.1016/j.tem.2020.07.001
738 (2020).
- 739 52 Howell, K. W. *et al.* Toll-like receptor 4 mediates oxidized LDL-induced macrophage
740 differentiation to foam cells. *J Surg Res* **171**, e27-31, doi:10.1016/j.jss.2011.06.033
741 (2011).
- 742 53 Csóka, B. *et al.* Adenosine promotes alternative macrophage activation via A2A and A2B
743 receptors. *Faseb j* **26**, 376-386, doi:10.1096/fj.11-190934 (2012).

- 744 54 Timblin, G. A. *et al.* Coenzyme A governs proinflammatory macrophage metabolism.
745 *bioRxiv*, 2022.2008.2030.505732, doi:10.1101/2022.08.30.505732 (2022).
- 746 55 Romero, A. & Peri, F. Increasing the Chemical Variety of Small-Molecule-Based TLR4
747 Modulators: An Overview. *Front Immunol* **11**, 1210, doi:10.3389/fimmu.2020.01210
748 (2020).
- 749 56 Rifkin, I. R., Leadbetter, E. A., Busconi, L., Viglianti, G. & Marshak-Rothstein, A. Toll-like
750 receptors, endogenous ligands, and systemic autoimmune disease. *Immunol Rev* **204**,
751 27-42, doi:10.1111/j.0105-2896.2005.00239.x (2005).
- 752 57 Midwood, K. *et al.* Tenascin-C is an endogenous activator of Toll-like receptor 4 that is
753 essential for maintaining inflammation in arthritic joint disease. *Nat Med* **15**, 774-780,
754 doi:10.1038/nm.1987 (2009).
- 755 58 Okamura, Y. *et al.* The extra domain A of fibronectin activates Toll-like receptor 4. *J Biol*
756 *Chem* **276**, 10229-10233, doi:10.1074/jbc.M100099200 (2001).
- 757 59 Lancaster, G. I. *et al.* Evidence that TLR4 Is Not a Receptor for Saturated Fatty Acids but
758 Mediates Lipid-Induced Inflammation by Reprogramming Macrophage Metabolism. *Cell*
759 *Metab* **27**, 1096-1110.e1095, doi:10.1016/j.cmet.2018.03.014 (2018).
- 760 60 Williamson, J. R. & Corkey, B. E. Assay of citric acid cycle intermediates and related
761 compounds--update with tissue metabolite levels and intracellular distribution. *Methods*
762 *Enzymol* **55**, 200-222, doi:10.1016/0076-6879(79)55025-3 (1979).
- 763 61 Cruz, C. M. *et al.* ATP activates a reactive oxygen species-dependent oxidative stress
764 response and secretion of proinflammatory cytokines in macrophages. *J Biol Chem* **282**,
765 2871-2879, doi:10.1074/jbc.M608083200 (2007).
- 766 62 Vénéreau, E., Ceriotti, C. & Bianchi, M. E. DAMPs from Cell Death to New Life. *Front*
767 *Immunol* **6**, 422, doi:10.3389/fimmu.2015.00422 (2015).
- 768 63 Gordon, S. & Martinez, F. O. Alternative Activation of Macrophages: Mechanism and
769 Functions. *Immunity* **32**, 593-604, doi:https://doi.org/10.1016/j.immuni.2010.05.007
770 (2010).
- 771 64 Ruffell, B., Affara, N. I. & Coussens, L. M. Differential macrophage programming in the
772 tumor microenvironment. *Trends Immunol* **33**, 119-126, doi:10.1016/j.it.2011.12.001
773 (2012).
- 774 65 Arnold, L. *et al.* Inflammatory monocytes recruited after skeletal muscle injury switch into
775 antiinflammatory macrophages to support myogenesis. *J Exp Med* **204**, 1057-1069,
776 doi:10.1084/jem.20070075 (2007).
- 777 66 Hesketh, M., Sahin, K. B., West, Z. E. & Murray, R. Z. Macrophage Phenotypes Regulate
778 Scar Formation and Chronic Wound Healing. *Int J Mol Sci* **18**, doi:10.3390/ijms18071545
779 (2017).
- 780 67 Lucas, T. *et al.* Differential Roles of Macrophages in Diverse Phases of Skin Repair. *The*
781 *Journal of Immunology* **184**, 3964-3977, doi:10.4049/jimmunol.0903356 (2010).
- 782 68 Major, J., Fletcher, J. E. & Hamilton, T. A. IL-4 pretreatment selectively enhances cytokine
783 and chemokine production in lipopolysaccharide-stimulated mouse peritoneal
784 macrophages. *J Immunol* **168**, 2456-2463, doi:10.4049/jimmunol.168.5.2456 (2002).
- 785 69 O'Brien, E. M. & Spiller, K. L. Pro-inflammatory polarization primes Macrophages to
786 transition into a distinct M2-like phenotype in response to IL-4. *J Leukoc Biol* **111**, 989-
787 1000, doi:10.1002/jlb.3a0520-338r (2022).
- 788 70 Liu, S. X., Gustafson, H. H., Jackson, D. L., Pun, S. H. & Trapnell, C. Trajectory analysis
789 quantifies transcriptional plasticity during macrophage polarization. *Sci Rep* **10**, 12273,
790 doi:10.1038/s41598-020-68766-w (2020).
- 791 71 Rao, A. J. *et al.* Revision joint replacement, wear particles, and macrophage polarization.
792 *Acta Biomater* **8**, 2815-2823, doi:10.1016/j.actbio.2012.03.042 (2012).
- 793 72 Dang, E. V. *et al.* Secreted fungal virulence effector triggers allergic inflammation via
794 TLR4. *Nature* **608**, 161-167, doi:10.1038/s41586-022-05005-4 (2022).

- 795 73 Faas, M. *et al.* IL-33-induced metabolic reprogramming controls the differentiation of
796 alternatively activated macrophages and the resolution of inflammation. *Immunity* **54**,
797 2531-2546.e2535, doi:10.1016/j.immuni.2021.09.010 (2021).
- 798 74 Kusnadi, A. *et al.* The Cytokine TNF Promotes Transcription Factor SREBP Activity and
799 Binding to Inflammatory Genes to Activate Macrophages and Limit Tissue Repair.
800 *Immunity* **51**, 241-257.e249, doi:10.1016/j.immuni.2019.06.005 (2019).
- 801 75 Ming-Chin Lee, K. *et al.* Type I interferon antagonism of the JMJD3-IRF4 pathway
802 modulates macrophage activation and polarization. *Cell Rep* **39**, 110719,
803 doi:10.1016/j.celrep.2022.110719 (2022).
- 804 76 Hsieh, W. Y., Williams, K. J., Su, B. & Bensinger, S. J. Profiling of mouse macrophage
805 lipidome using direct infusion shotgun mass spectrometry. *STAR Protoc* **2**, 100235,
806 doi:10.1016/j.xpro.2020.100235 (2021).
- 807 77 Divakaruni, A. S., Paradyse, A., Ferrick, D. A., Murphy, A. N. & Jastroch, M. Analysis and
808 interpretation of microplate-based oxygen consumption and pH data. *Methods Enzymol*
809 **547**, 309-354, doi:10.1016/b978-0-12-801415-8.00016-3 (2014).
- 810 78 Divakaruni, A. S. & Jastroch, M. A practical guide for the analysis, standardization and
811 interpretation of oxygen consumption measurements. *Nat Metab* **4**, 978-994,
812 doi:10.1038/s42255-022-00619-4 (2022).
- 813 79 Desousa, B. R. *et al.* Calculation of ATP production rates using the Seahorse XF Analyzer.
814 *EMBO Rep* **24**, e56380, doi:10.15252/embr.202256380 (2023).
- 815 80 Cordes, T. & Metallo, C. M. Quantifying Intermediary Metabolism and Lipogenesis in
816 Cultured Mammalian Cells Using Stable Isotope Tracing and Mass Spectrometry.
817 *Methods Mol Biol* **1978**, 219-241, doi:10.1007/978-1-4939-9236-2_14 (2019).
- 818 81 Trefely, S., Ashwell, P. & Snyder, N. W. FluxFix: automatic isotopologue normalization for
819 metabolic tracer analysis. *BMC Bioinformatics* **17**, 485, doi:10.1186/s12859-016-1360-7
820 (2016).
- 821 82 Argus, J. P. *et al.* Development and Application of FASA, a Model for Quantifying Fatty
822 Acid Metabolism Using Stable Isotope Labeling. *Cell Rep* **25**, 2919-2934.e2918,
823 doi:10.1016/j.celrep.2018.11.041 (2018).
- 824 83 Ramírez, F. *et al.* deepTools2: a next generation web server for deep-sequencing data
825 analysis. *Nucleic Acids Res* **44**, W160-165, doi:10.1093/nar/gkw257 (2016).
- 826 84 Robinson, M. D., McCarthy, D. J. & Smyth, G. K. edgeR: a Bioconductor package for
827 differential expression analysis of digital gene expression data. *Bioinformatics* **26**, 139-
828 140, doi:10.1093/bioinformatics/btp616 (2010).
- 829 85 Love, M. I., Huber, W. & Anders, S. Moderated estimation of fold change and dispersion
830 for RNA-seq data with DESeq2. *Genome Biol* **15**, 550, doi:10.1186/s13059-014-0550-8
831 (2014).
- 832 86 Subramanian, A. *et al.* Gene set enrichment analysis: a knowledge-based approach for
833 interpreting genome-wide expression profiles. *Proc Natl Acad Sci U S A* **102**, 15545-
834 15550, doi:10.1073/pnas.0506580102 (2005).
- 835 87 Korotkevich, G. *et al.* Fast gene set enrichment analysis. *bioRxiv*, 060012,
836 doi:10.1101/060012 (2021).
- 837 88 Liberzon, A. *et al.* The Molecular Signatures Database (MSigDB) hallmark gene set
838 collection. *Cell Syst* **1**, 417-425, doi:10.1016/j.cels.2015.12.004 (2015).
- 839 89 Dolgalev, I. Vol. R package version 7.5.1.9001 (2022).
- 840

841

842 **FIGURE LEGENDS**

843 **Figure 1. Exogenous CoA provision enhances alternative macrophage activation**
844 **(a)** qPCR analysis of the IL-4-associated genes *Mgl2*, *Pdcd1gl2*, *Chil4*, *Ccl8*, and *Fizz1* in BMDMs
845 treated with CoA (1 mM), IL-4 (20 ng/mL), CoA + IL-4, or vehicle for 48 hr. (n≥9 independent
846 biological replicates). **(b-d)** Flow cytometric analysis of the IL-4-associated cell surface markers
847 CD206, CD301, and CD71 after treatments as in (a). (b) Contour plots with the percentage of
848 cells expressing both CD206 and CD301 is indicated in the upper right quadrant. Data shown are
849 from a single representative experiment. (c) Aggregate mean fluorescence intensity of CD206,
850 CD301, and CD71 (n=9 independent biological replicates). (d) Percentage of CD206⁺/CD301⁺
851 and CD206⁺/CD71⁺ populations (n=9 independent biological replicates). **(e)** Representative
852 images of BMDMs incubated for 1 hr. with FITC-Dextran (1mg/mL, green) and Hoechst 3342
853 (10ng/mL, blue) after stimulation with compounds as in (a). **(f)** Aggregate image analysis data for
854 experiments as in (e) (n=3 independent biological replicates). **(G)** Quantification of CD206⁺/CD71⁺
855 peritoneal macrophages from mice that were exposed to vehicle (PBS), CoA (40mg/kg), IL-4c (5
856 µg IL-4 and 25 µg anti-IL-4 monoclonal antibody), or the combination of IL-4c + CoA. (n≥3 mice
857 were used for each group). All data are presented as mean ± SEM. *p < 0.05; **p < 0.01; ***p <
858 0.001.

859
860 **Figure 2: CoA does not enhance alternative macrophage activation by boosting known**
861 **metabolic hallmarks of the IL-4 response.**

862 **(a)** Intracellular levels of CoA and acetyl CoA in BMDMs measured by LC-MS/MS. Cells were
863 treated with IL-4 (20 ng/mL), IL-4 + CoA (1 mM), or vehicle for 48 hr. as in Fig. 1 (n=3 independent
864 biological replicates). **(b)** Representative respirometry trace of BMDMs treated as in (a). (n=5
865 technical replicates from a single biological replicate). **(c)** Aggregate ATP-linked and FCCP-
866 stimulated respiration in intact BMDMs for treatments as in (a). Cells were offered 8 mM glucose,
867 2 mM pyruvate, and 2 mM glutamine in the experimental medium (n=8 independent biological
868 replicates). **(d)** Lactate efflux rate from respirometry experiments in (b & c) calculated using
869 Seahorse XF data and correcting for respiratory CO₂ (n=8 independent biological replicates). **(e)**
870 Metabolite abundances of citrate, α-ketoglutarate(α-KG), and malate in BMDMs treated as in (a)
871 (n=7 independent biological replicates). **(f)** Enrichment from uniformly labeled ¹³C₆-glucose into
872 the TCA cycle intermediates as in (e) (n=8 independent biological replicates). **(g)** Quantification
873 of newly synthesized palmitic acid (16:0) and palmitoleic acid (16:1) from BMDMs stimulated as
874 in (a). (data shown as n=8 technical replicates from n=2 independent biological replicates). **(h)**
875 Schematic depicting the mechanism of action of cyclopropane carboxylic acid (CPCA) and PZ-
876 2891. **(i)** Intracellular CoA levels of BMDMs stimulated with IL-4, IL-4 + CPCA (1 mM), or IL-4+PZ-
877 2891 (10 µM) for 48 h (n=5 independent biological replicates). **(j)** Flow cytometric quantification
878 of the CD206⁺/CD301⁺ population for BMDMs treated as in (i) (n=5 independent biological
879 replicates). All data are presented as mean ± SEM. *p < 0.05; **p < 0.01; ***p < 0.001.

880
881

882 **Figure 3. Exogenous CoA induces a pro-inflammatory response in BMDMs**

883 **(a)** Volcano plot from bulk RNA sequencing data from BMDMs treated IL-4 (20 ng/mL), IL-4 + 1
884 mM CoA, or vehicle control for 48 hr. comparing differential gene expression between IL-4 vs.
885 vehicle controls (left) and IL-4 + CoA vs. IL-4 (right). Genes associated with classical activation
886 are depicted in red, genes associated with alternative activation are shown in blue. **(b)** Gene Set
887 Enrichment Analysis of genes upregulated in BMDMs treated with IL-4+CoA vs. IL-4 alone. **(c)**
888 qPCR analysis of *I11b*, *Tnf*, *Irg1*, and *Nos2* in BMDMs stimulated with CoA (1mM) or vehicle
889 control for 4 hr. (n=4 independent biological replicates). **(d)** qPCR analysis of the interferon-
890 stimulated gene *Mx1* in BMDMs stimulated with 1 mM CoA or vehicle control for 24 hr. (n=4
891 independent biological replicates). **(e)** Itaconate abundance after treatment with 1 mM CoA or
892 vehicle control for 48 hr. (n=6 independent biological replicates). **(f)** qPCR analysis of *I11b* and
893 *Tnf* in the peritoneal exudate cells of mice treated with (40 mg/kg) CoA 6 hr. prior to collection

894 (n≥5 mice for each group). **(g)** Quantification of cytokines in the peritoneal lavage fluid (PLF) of
895 mice treated as in (g) using Multiplexed ELISA (n=3 mice were used for each group). All data are
896 presented as mean ± SEM. *p < 0.05; **p < 0.01.

897

898 **Figure 4. CoA is a TLR4 agonist**

899 **(a)** qPCR analysis of *Il1b*, *Tnf*, *Irg1*, *I12b*, and *Nos2* in WT and *Myd88*^{-/-} BMDMs stimulated with
900 1 mM CoA or vehicle control for 4 hr. (n≥3 independent biological replicates). **(b)** Concentration-
901 response curve of linked alkaline phosphatase activity in hTLR4 reporter cells with varying
902 concentrations of LPS (black dots). The red dot and dashed lines represent the OD₆₃₀ observed
903 in response to 1 mM CoA treatment (n=4 independent biological replicates). **(c)** Aggregated
904 response of 1 mM CoA compared to vehicle control in hTLR2, hTLR4, and hTLR7 relative to
905 maximum TLR activation. (n≥3 independent biological replicates). **(d)** qPCR analysis of *Il1b*, *Tnf*,
906 *I12b*, and *Nos2* in WT and *Tlr4*^{-/-} BMDMs following treatment with 1 mM CoA for 4 hr. (n=3
907 independent biological replicates). **(e)** Abundance of itaconate in WT, *Myd88*^{-/-}, and *Tlr4*^{-/-} BMDMs
908 in response to 1 mM CoA treatment for 48 hr. or vehicle control (n≥5 independent biological
909 replicates). All data are presented as mean ± SEM. *p < 0.05; ***p < 0.001.

910

911 **Figure 5. Myd88-linked TLR-ligands enhance IL-4 the response**

912 **(a-b)** Flow cytometric analysis of CD206 and CD301 in BMDMs stimulated for 48 hr. with vehicle
913 control, IL-4 (20 ng/mL), or IL-4 in combination with one of the following: LPS (0.1 ng/mL),
914 Pam3CSK4 (5ng/mL), Imiquimod (10 μM), Flagellin (100 ng/mL), or Poly (I:C) (1 μg/mL) (a)
915 Contour plots showing the percentage of cells expressing both CD206 and CD301 in the upper
916 right quadrant. Data are from a single representative experiment. (b) Percentage of
917 CD206⁺/CD301⁺ populations for treatments as in (a) (n=8 independent biological replicates). **(c)**
918 qPCR analysis of *Mgl2* and *Ym1* in BMDMs stimulated with vehicle control, IL-4, or IL-4 in
919 combination with LPS, Pam3CSK4, or Poly (I:C) for 48h. Concentrations as in (a) (n≥3
920 independent biological replicates). **(d)** Aggregate FITC⁺ foci per cell for BMDMs stained with FITC-
921 Dextran and treated as with vehicle control, IL-4, or IL-4 with either LPS or Pam3CSK4 as in (a).
922 (n=4 independent biological replicates). **(e)** Percentage of CD206⁺/CD301⁺ populations in WT and
923 *Myd88*^{-/-} BMDMs stimulated with vehicle control, IL-4, or IL-4 with either LPS or Pam3CSK4 as in
924 (a) (n=8 independent biological replicates). **(f)** qPCR analysis of *Mgl2* and *Ym1* for BMDMs as in
925 (e) (n=4 independent biological replicates). **(g)** Quantification of CD206⁺/CD71⁺ peritoneal
926 macrophages from mice that were injected with vehicle control, IL-4c (5 μg IL-4 and 25 μg anti-
927 IL-4 monoclonal antibody), IL-4c + LPS (125 μg), IL-4c + Pam3CSK4 (50 μg), or IL-4c + Poly (I:C)
928 (200 μg). (n≥9 mice were used for each group). **(h)** Weights of subcutaneous B16-F10 melanoma
929 tumors that were derived from the co-implantation of B16-F10 tumor cells and BMDMs that were
930 stimulated with either vehicle control, IL-4, or IL-4 in combination with Pam3CSK4. All data are
931 presented as mean ± SEM. *p < 0.05; **p < 0.01; ***p < 0.001; ns, not significant.

932

933 **Figure 6. MyD88-linked signaling increases chromatin accessibility in IL-4-stimulated 934 macrophages**

935 **(a)** Heatmap of z-scored ATAC-seq signal for the 10,878 IL-4-inducible regions. The heatmap is
936 arranged by increasing values for IL-4 with Pam3CSK4 co-treatment group and is divided into 10
937 equal bins. Side bar indicates distance to closest transcription start site (TSS). **(b)** Heatmap
938 showing p-values of the most highly enriched motifs for each of the 10 bins that were generated
939 in (a). **(c)** Top 3 hits from de novo transcription factor motif analysis on the significantly induced
940 regions by Pam3CSK4 co-treatment (log₂ fold change >0.5, false discovery rate < 0.05). **(d)**
941 Representative tracks of *Chil4* and *Ccl8* promoter regions with nearby c-Jun/AP-1 motifs.

942

Figure 1

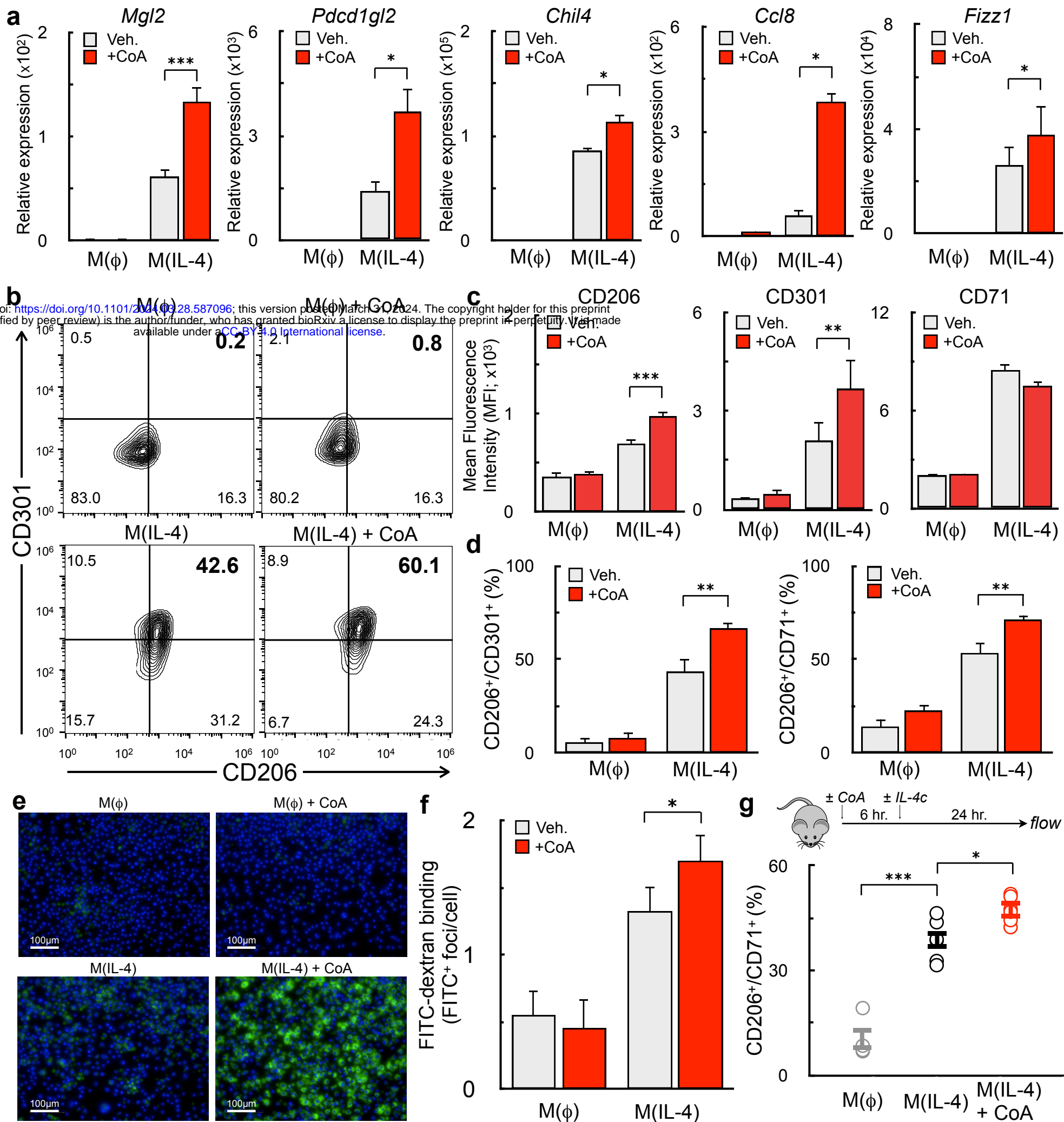


Figure 2

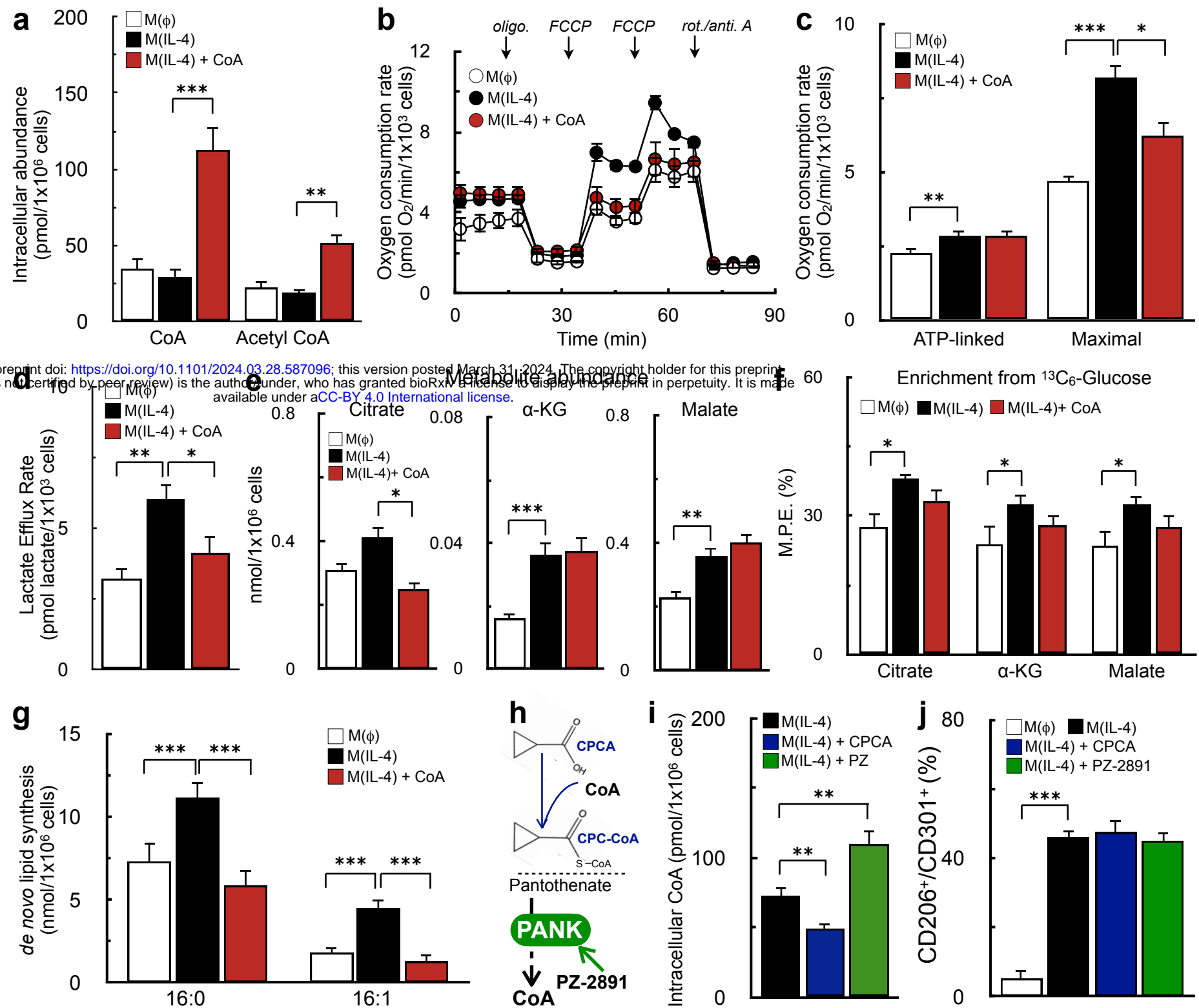


Figure 3

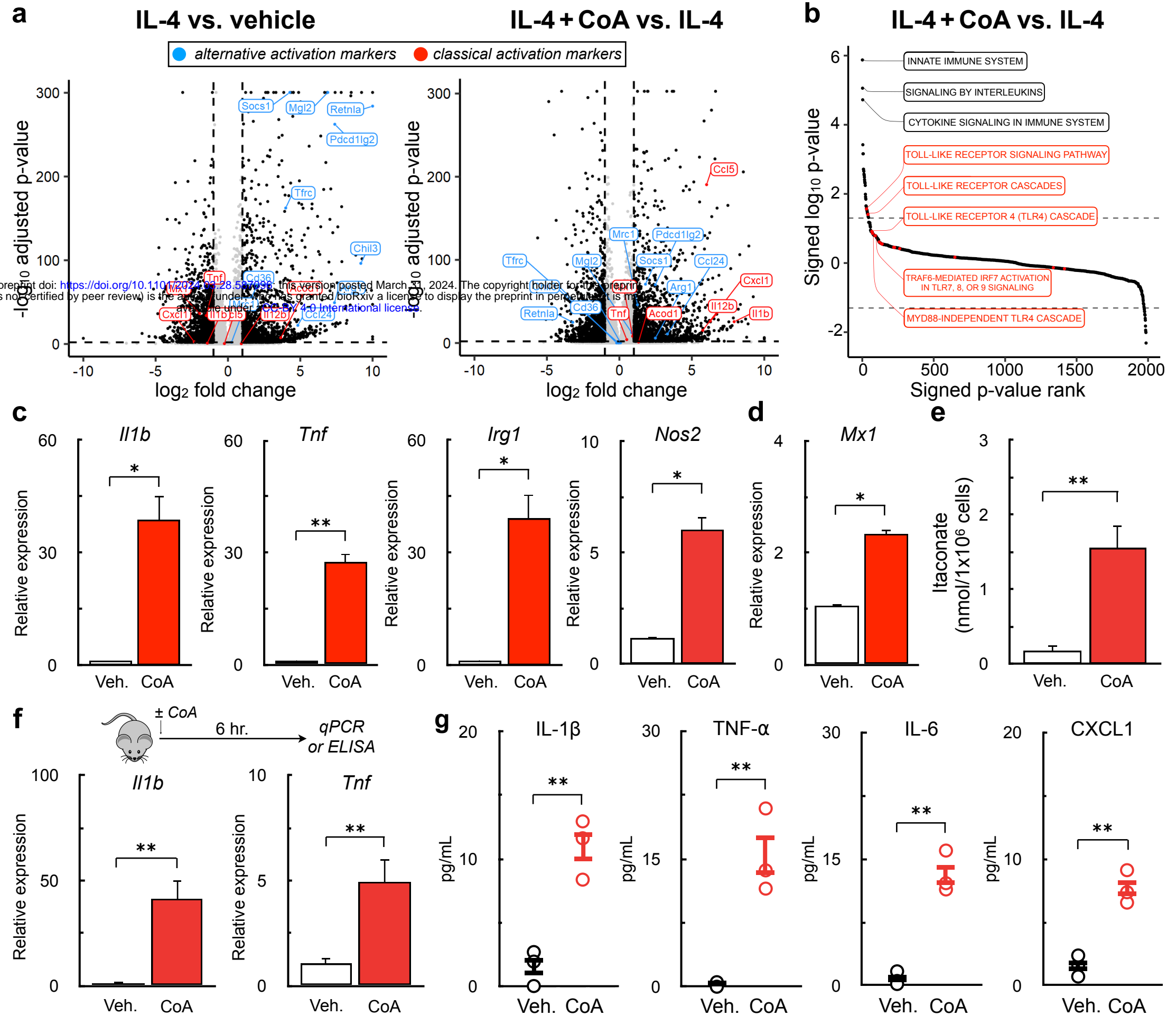
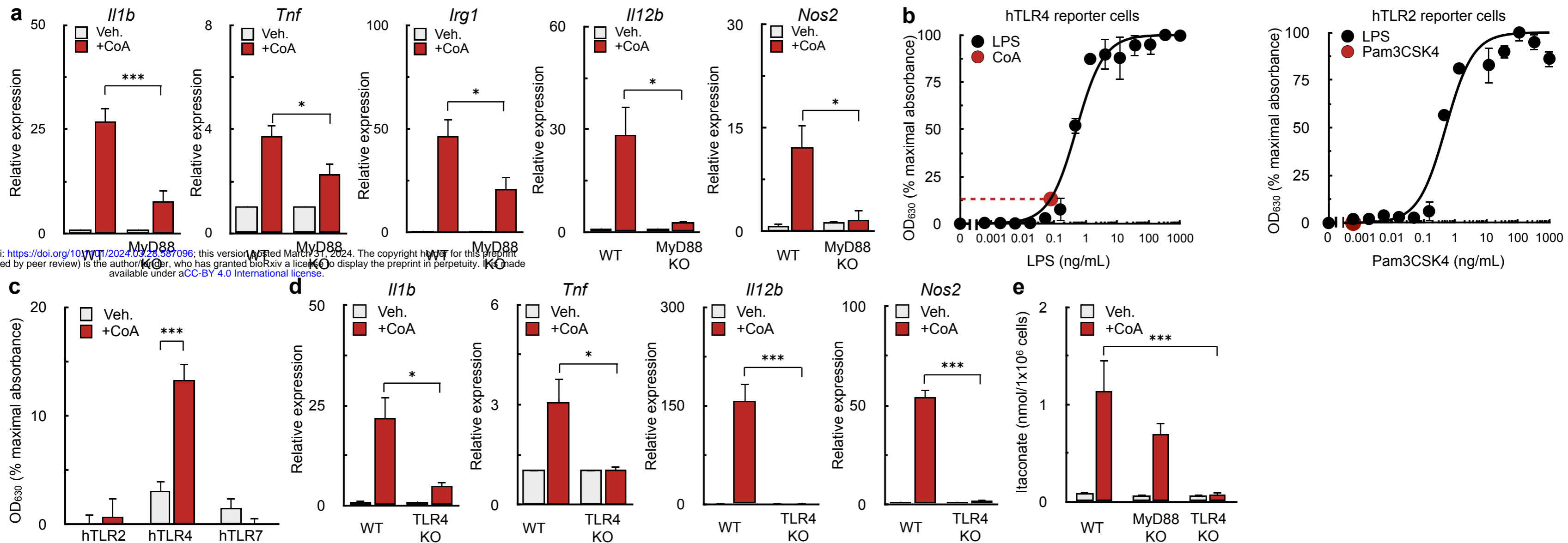


Figure 4



https://doi.org/10.1101/2024.03.28.587096; this version posted March 31, 2024. The copyright holder for this preprint (which was not certified by peer review) is the author/funder, who has granted bioRxiv a license to display the preprint in perpetuity. It is made available under aCC-BY 4.0 International license.

Figure 5

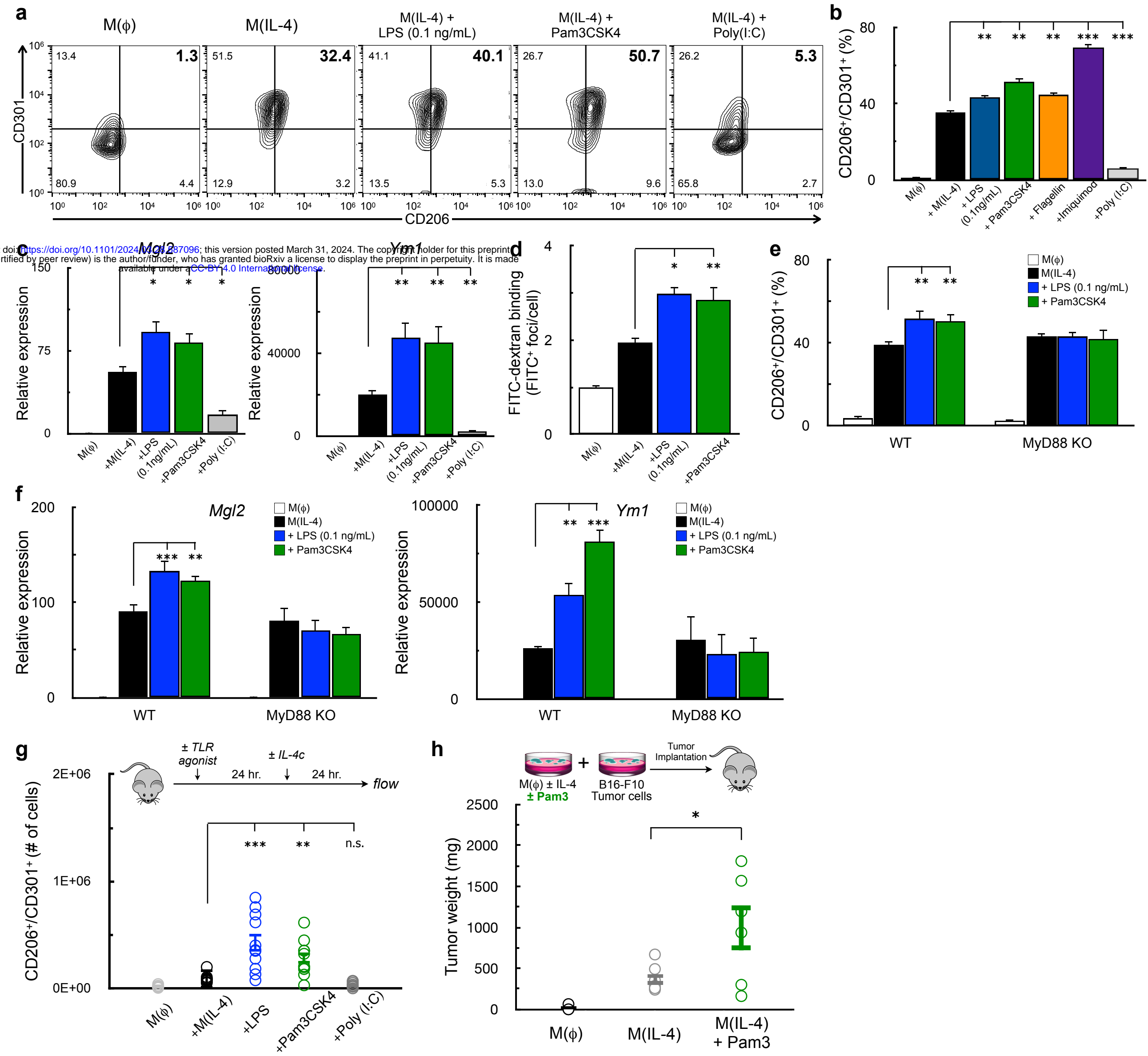
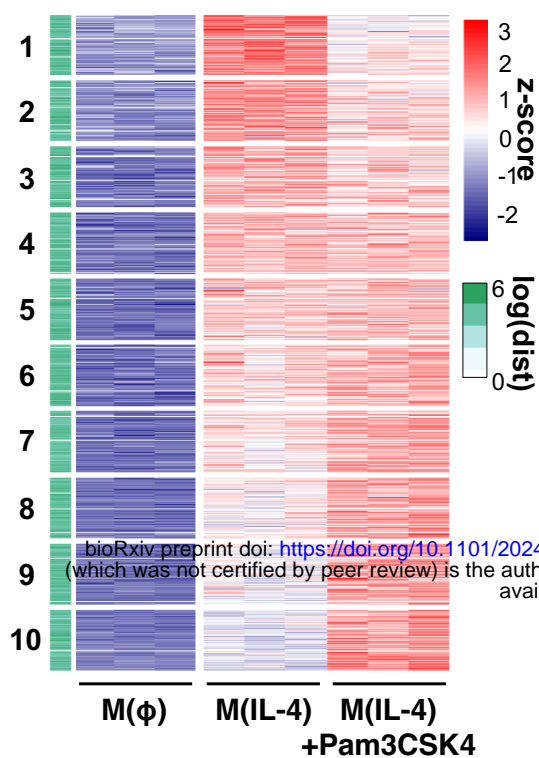
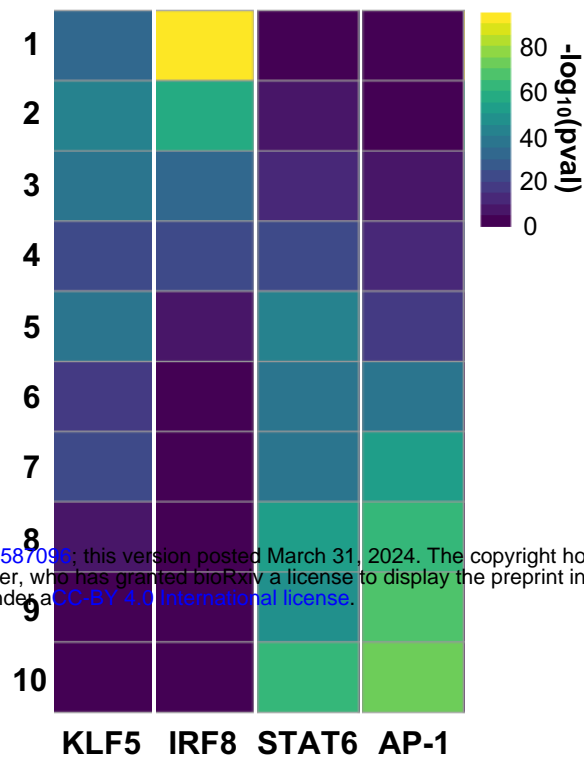


Figure 6

a



b



bioRxiv preprint doi: <https://doi.org/10.1101/2024.03.28.587096>; this version posted March 31, 2024. The copyright holder for this preprint (which was not certified by peer review) is the author/funder, who has granted bioRxiv a license to display the preprint in perpetuity. It is made available under aCC-BY 4.0 International license.

c

| De novo motif | Best Match | % Targets | $-\log_{10}(\text{pval})$ |
|---------------|--------------------|-----------|---------------------------|
| | <i>Fra1</i> (bZIP) | 61 | 144 |
| | <i>Stat6</i> | 31 | 108 |
| | <i>Egr2</i> | 21 | 47 |

d

